

---

# Spiking Transformer with Spatial-Temporal Attention

---

**Donghyun Lee**  
Yale University  
donghyun.lee@yale.edu

**Yuhang Li**  
Yale University  
yuhang.li@yale.edu

**Youngeun Kim**  
Yale University  
youngeun.kim@yale.edu

**Shiting Xiao**  
Yale University  
ginny.xiao@yale.edu

**Priyadarshini Panda**  
Yale University  
priya.panda@yale.edu

## Abstract

Spiking Neural Networks (SNNs) present a compelling and energy-efficient alternative to traditional Artificial Neural Networks (ANNs) due to their sparse binary activation. Leveraging the success of the transformer architecture, the spiking transformer architecture is explored to scale up dataset size and performance. However, existing works only consider the spatial self-attention in spiking transformer, neglecting the inherent temporal context across the timesteps. In this work, we introduce Spiking Transformer with **Spatial-Temporal Attention (STAtten)**, a simple and straightforward architecture designed to integrate spatial and temporal information in self-attention with negligible additional computational load. The STAtten divides the temporal or token index and calculates the self-attention in a cross-manner to effectively incorporate spatial-temporal information. We first verify our spatial-temporal attention mechanism’s ability to capture long-term temporal dependencies using sequential datasets. Moreover, we validate our approach through extensive experiments on varied datasets, including CIFAR10/100, ImageNet, CIFAR10-DVS, and N-Caltech101. Notably, our cross-attention mechanism achieves an accuracy of 78.39 % on the ImageNet dataset.

## 1 Introduction

Spiking Neural Networks (SNNs) are emerging as a bio-inspired alternative to conventional Artificial Neural Networks (ANNs) [1, 2]. Operating through sparse binary computation, SNN’s unique spike-driven mechanism not only holds the promise of energy-efficient computing but also extends its applicability across various computing platforms such as TrueNorth [3], Loihi [4], and Tianjic [5]. SNNs are typically designed by using convolution-based architectures, such as VGGNet [6, 7] and ResNet [8, 9], which achieve computational efficiency benefit. However, convolution-based SNN architectures often suffer from poor performance compared to ANNs due to information loss stemming from binary activations.

To handle this problem, inspired by the huge success of transformers [10–13], spike-formed transformers have emerged in SNNs to boost capacity with energy-efficient computation in various tasks, *e.g.*, object tracking [14], computer vision [15, 16], depth estimation [17], and speech recognition [18, 19]. Specifically, in the computer vision domain, Spikformer [15] and Spike-driven Transformer (SDT) [16] propose spike-formed self-attention, *i.e.*, query ( $Q$ ), key ( $K$ ), and value ( $V$ ) without Softmax function, resulting in energy-efficient computation.

However, even though the SNN architecture inherently harnesses the temporal information across the membrane potential of Leaky-and-Integrated (LIF) neurons [20, 21], previous spiking transformers have not fully utilized the temporal correlation in the attention mechanism [15, 16] as shown in Fig.

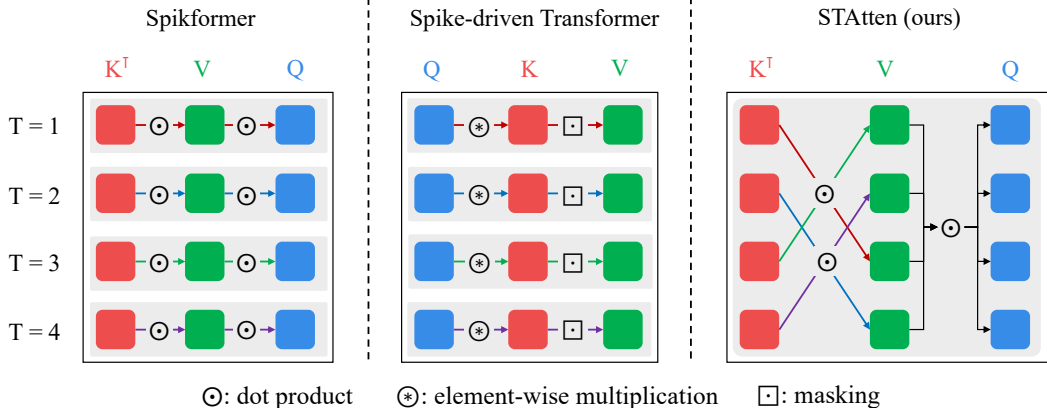


Figure 1: Self-attention mechanism of Spikformer [15], Spike-driven Transformer (SDT) [16], and STAtten. Query ( $Q$ ), key ( $K$ ), and value ( $V$ ) are spike-formed. In Spikformer and SDT, the self-attention operates independently across timesteps. In contrast, our STAtten aggregates information across timesteps, enabling integration of spatial and temporal context.

1. Furthermore, our observations indicate that the similarity of spike patterns in  $K$  and  $V$  varies across timesteps shown in Fig. 2, underscoring the need for incorporating temporal correlation in self-attention mechanisms.

In this work, we propose Spiking Transformer with **Spatial-Temporal Attention (STAtten)**, designed to properly integrate temporal and spatial information. In [22, 12], they have proposed various attention methods which correlate every token in the spatial-temporal dimension jointly. However, it suffers from quadratic computational complexity with respect to the number of tokens and video frames, *i.e.*,  $\mathcal{O}(T^2N^2D)$ , where  $T$  is timestep,  $N$  is the number of tokens, and  $D$  is channel dimension. Therefore, we present two simple cross-attention methods to reduce the computational complexity: **T-STAtten** and **N-STAtten**. The T-STAtten method partitions the tokens across timestep and computes self-attention across different temporal indexes. Similarly, in the N-STAtten method, we divide the tokens based on patch locations and calculate self-attention across different spatial indexes. In summary, the main contributions are as follows:

- We observe the necessity of spatial-temporal correlation in the self-attention mechanism of spiking transformers by analyzing the similarity of spike patterns between the components of self-attention.
- We propose three straightforward spatial-temporal attention modules for spiking transformers, effectively integrating spatial and temporal context into the self-attention mechanism with minimal additional computational burden.
- Our rigorous experiments verify our spatial-temporal self-attention on classification tasks across static and dynamic datasets, including CIFAR10/100, ImageNet, CIFAR10-DVS, and N-Caltech101. Specifically, our STAtten architecture achieves 78.11 % and 78.39 % accuracy on the ImageNet dataset with resolutions of  $224 \times 224$  and  $288 \times 288$ , respectively.

## 2 Related Works

**Spiking Convolutional Neural Network.** The advancements in SNNs have sparked considerable exploration into effective training and deployment methodologies based on convolution-based architecture. There are two primary approaches to training SNNs: ANN-to-SNN conversion and using a modified backpropagation method with surrogate gradients. The ANN-to-SNN conversion method involves adapting pre-trained ANNs into configurations suitable for SNNs. This approach aims to leverage the knowledge acquired from ANNs to expedite and enhance the performance of SNNs. Research like [23–26] have contributed significantly to this area by explaining the conversion process and showcasing how ANNs can serve as helpful guides for training SNNs. Backpropagation, a

common technique for training ANNs, has also been applied to SNNs with adjustments to accommodate the discrete nature of spike events. A key aspect of this approach is the use of surrogate gradients, which simplifies the incorporation of backpropagation methods into SNN training. Notable contributions from [27, 28, 8] have been instrumental in advancing our understanding of training techniques for SNNs. Furthermore, the direct training with surrogate gradients in SNNs has enabled convolution-based SNN architectures to achieve energy-efficient computation and superior performance compared to ANN-to-SNN conversion methods across various tasks, including image classification [8, 29, 9], semantic segmentation [30], and object detection [31].

**Spiking Transformer.** Although convolution-based SNNs enjoy energy-efficient computations, they often suffer from poor accuracy compared to ANN due to their sparse information representation. To address this, transformer architectures have been adapted to SNNs, leveraging their self-attention mechanisms and ability to capture long-range dependencies. This has led to the development of spike-formed transformer architectures like Spikformer [15] and the SDT [16], which aim to achieve high performance in SNNs. In Spikformer [15], they pioneer the implementation of SNN-based transformer and spike-formed self-attention mechanisms. They eliminate the Softmax function in the self-attention part for the following two reasons: (1)  $Q$ ,  $K$ , and  $V$  are already non-negative binary values, and (2) binarized  $Q$ ,  $K$ , and  $V$  do not need to be scaled by the Softmax function. Building upon Spikformer, [16] proposes the SDT, featuring a novel self-attention block incorporating masking and sparse addition to minimize power consumption. Furthermore, they rearrange the residual connections to transfer membrane potential rather than spikes, as demonstrated in MS-ResNet [9]. However, the existing self-attention in spiking transformers only considers the spatial domain. Our method, instead, proposes spatial-temporal attention to integrate spatial and temporal information simultaneously.

### 3 Preliminary

#### 3.1 Leaky Integrate-and-Fire Neuron

As a fundamental building block of SNNs, the LIF neuron [32] has emerged as an important component for energy-efficient computation. The LIF neuron is a non-linear activation function that determines whether neurons fire spikes as follows:

$$\mathbf{u}_{t+1}^l = \tau \mathbf{u}_t^l + \mathbf{W}^l f(\mathbf{u}_t^{l-1} - V_{th}) \quad (1)$$

$$f(\mathbf{u}_t^l - V_{th}) = \begin{cases} 1 & \text{if } \mathbf{u}_t^l > V_{th}, \\ 0 & \text{otherwise} \end{cases}, \quad (2)$$

where,  $\mathbf{u}_t^l$  is the membrane potential in  $l$ -th layer at timestep  $t$ ,  $\tau \in (0, 1]$  is the leaky factor for membrane potential leakage,  $\mathbf{W}^l$  is the weight of  $l$ -th layer, and  $f(\cdot)$  is the LIF function with firing threshold  $V_{th}$ . Therefore, when the membrane  $\mathbf{u}_t^l$  is higher than  $V_{th}$ , the LIF function fires a spike and the membrane potential is reset to 0.

#### 3.2 Vanilla self-attention

Inspired by the self-attention mechanism introduced in transformers for natural language processing [10], the Vision Transformer (ViT) [11] first attempts self-attention on the image dataset. The performance of transformer with the self-attention mechanism has surpassed convolution-based architectures due to its ability to capture global features through long-range dependency:

$$\mathbf{z} = \text{Softmax}\left(\frac{\mathbf{Q}\mathbf{K}^\top}{\sqrt{D}}\right)\mathbf{V}, \quad \mathbf{Q}, \mathbf{K}, \mathbf{V} \in \mathbb{R}^{N \times D}, \quad (3)$$

where  $N$  is the number of tokens and  $D$  is the channel dimension. Note that the computational complexity of attention is  $\mathcal{O}(N^2D)$  due to its matrix multiplication operation.

#### 3.3 Spike-driven Transformer

Our proposed methods are integrated into the SDT [16] architecture, serving as our baseline. Here we provide an overview of this baseline architecture. The SDT comprises four main components:

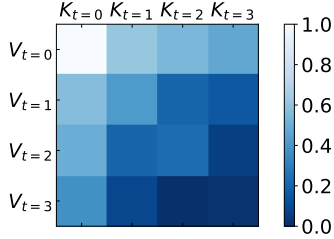


Figure 2: The normalized similarity of spike patterns between  $K$  and  $V$  in self-attention of SDT architecture. The white and blue colors represent high and low similarity respectively.

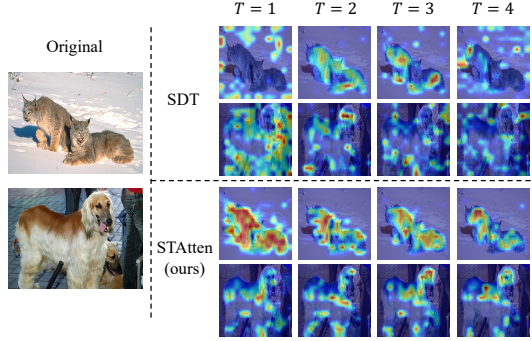


Figure 3: Grad-CAM [33] visualization of SDT and our proposed STAtten.

Spiking Patch Splitting, Spike-Driven Self-Attention, Multi-Layer Perceptron, and classification head. Within the Spiking Patch Splitting block, the input  $I \in \mathbb{R}^{T \times C \times H \times W}$  undergoes partitioning into  $N$  patches, where  $T$  is timestep,  $C$  is channel dimension, and  $H, W$  denote height and width of the 2D image input, respectively. Following the Spiking Patch Splitting block, the split patches proceed sequentially through self-attention to extract and mix feature information from the embedded tokens. In self-attention calculation, Hadamard product and masking are utilized as shown in Fig. 1, enabling low power consumption in this part. Furthermore, they modify the residual connection location before the LIF neuron, which transfers the membrane potential, to prevent information loss and manage multi-bit spikes. However, while every component of the SDT, except for self-attention, effectively integrates information across timesteps due to the LIF neurons, self-attention exclusively considers only spatial attention for token information mixing. In the following section, we introduce three spatial-temporal self-attention modules aimed at fully harnessing spatial and temporal information. A more detailed explanation of the SDT architecture is provided in Appendix A.

## 4 Methodology

In this section, we present our observations in the spiking transformer and detail our methodology. We first introduce the motivations for incorporating spatial-temporal attention in spiking transformers, including the similarity of spike patterns and Grad-CAM [33] visualizations. We then propose our spatial-temporal attention methods.

### 4.1 Motivation of Spatial-Temporal Attention

SNNs typically utilize LIF neurons to convert membrane potentials into binary activations over multiple timesteps. This results in spike-formed feature maps with each timestep, reflecting a distinct distribution of membrane potentials influenced by the leaky factor and reset function. Consequently, spike information varies across timesteps. Inspired by [34], which highlights the different class probabilities from different timesteps, we further investigate the temporal dynamics within the self-attention of spiking transformers. Using a pre-trained model of the SDT [16], we extract the spike patterns of  $K$  and  $V$ , which are used for attention calculation, over 4 timesteps on the sampled ImageNet dataset to measure their similarity. The similarity is computed using the Hamming distance between two spike patterns across all encoder layers, indicating the extent of variation in spikes across timesteps. Fig. 2 illustrates the normalized similarity of spike patterns between  $K$  and  $V$  across all timesteps, where white and blue colors represent high and low similarity, respectively. The diagonal components of Fig. 2 correspond to spatial domain correlation, which has been considered in previous works [15, 16], while the off-diagonal components represent the correlation across the temporal domain. Our findings reveal that temporal similarities between  $K$  and  $V$  decrease as timesteps increase, as do spatial similarities, indicating various correlated patterns across the timesteps.

We further present the Grad-CAM [33] visualizations of the SDT and our STAtten methods to validate the capability of spatial-temporal attention in spiking transformers. As shown in Fig. 3, our STAtten method demonstrates consistent object recognition across timesteps, whereas SDT inconsistently captures the object, sometimes focusing on the background in specific timesteps. Additionally, our

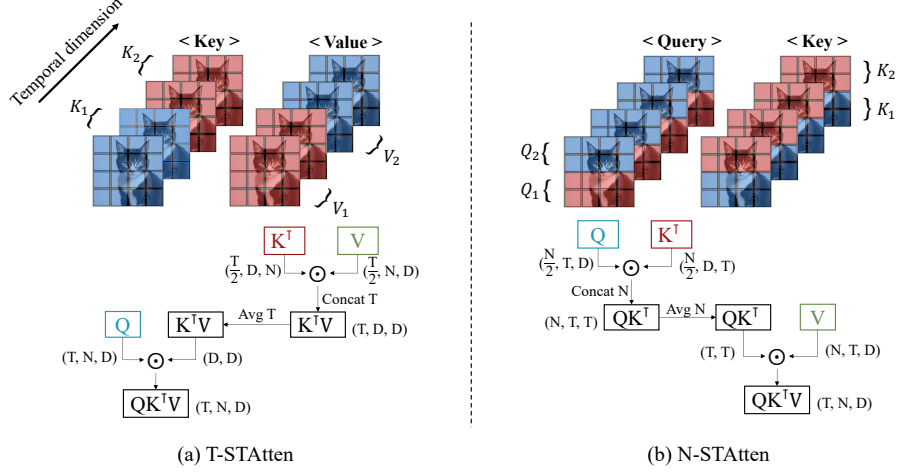


Figure 4: Spatial-temporal self-attention methods. Every  $Q$ ,  $K$ , and  $V$  is spike-formed and the Softmax function is not needed. (a) STAtten:  $K$  and  $V$  are divided into two groups across timestep and attention is calculated between tokens with different timesteps. (b) N-STAtten:  $Q$  and  $K$  are divided into two groups each across the location of patches and attention score is obtained between tokens across a different index of patches. Note that  $T$ ,  $N$ , and  $D$  are timestep, the number of tokens, and channel dimension respectively, and  $\odot$  represents the dot product. We provide the tensor shapes of  $Q$ ,  $K$ , and  $V$ , which are reshaped and transposed to proceed the matrix multiplication.

STAtten method captures a more comprehensive global range of the target object compared to SDT. These observations highlight the necessity of incorporating spatial-temporal attention to effectively capture and leverage diverse information across timesteps within spiking transformers.

## 4.2 STAtten

In this section, we introduce three spatial-temporal attention modules tailored for the spiking transformer architecture. We present two cross-attention methods: T-STAtten and N-STAtten, which calculate attention across different timesteps and token locations, respectively. The overall scheme of the spatial-temporal attention is illustrated in Fig. 4. Note that the tensor sizes of  $Q$ ,  $K$ , and  $V$  in spiking transformer are  $\mathbb{R}^{T \times N \times D}$ .

**T-STAtten.** In the SNN-based transformer, since the Softmax function is no longer required due to the spike-formed multiplication [15], we can freely adjust the order of  $Q$ ,  $K$ , and  $V$  multiplication in self-attention as follows:  $Q \odot (K^\top \odot V)$ , resulting in a more efficient computational complexity like  $\mathcal{O}(TND^2)$ . As illustrated in Fig. 4(b), T-STAtten applies cross attention between  $K$  and  $V$  to effectively integrate spatial-temporal information. We first divide the  $K$  and  $V$  into two groups across the timestep, denoted as  $K_1, K_2$  for key and  $V_1, V_2$  for value. Subsequently, we calculate the attention matrix between the keys and values with different timestep indexes. For example, with 4 timesteps, we compute the self-attention between keys at  $t = 1, 2$  and values at  $t = 3, 4$ . To aggregate the attention information, we average the output of cross-attention across timesteps. Finally, the averaged attention is multiplied by the  $Q$  to obtain the final output, which is then converted to spikes by LIF neurons. The formulation for T-STAtten is as follows:

$$C_1 = (K_1^\top \odot V_2), C_2 = (K_2^\top \odot V_1), \quad C_{1,2} \in \mathbb{R}^{\frac{T}{2} \times D \times D} \quad (4)$$

$$\text{Attn} = \text{Avg}_t(\text{Concat}_t(C_1, C_2)) \quad \text{Attn} \in \mathbb{R}^{D \times D} \quad (5)$$

$$O = \alpha \cdot (Q \odot \text{Attn}) \quad O \in \mathbb{R}^{T \times N \times D}, \quad (6)$$

where  $\odot$  is the dot product,  $\text{Avg}_t$  and  $\text{Concat}_t$  represent averaging and concatenate function across the temporal dimension respectively,  $\alpha$  is scaling factor, and  $O$  means the final output of spatial-temporal attention block.

**N-STAtten.** To further decrease the computational complexity with sustaining spatial-temporal mixing in self-attention, the N-STAtten partitions the  $Q$  and  $K$  into two groups based on the

Table 1: Computational complexity and energy consumption comparison of the various self-attention methods. The  $E_{MAC}$  represents the energy cost for multiply-accumulate operation (MAC),  $E_{AC}$  is for accumulate operation (AC),  $N$  is the number of patches,  $D$  is the hidden dimension,  $T$  is the timestep.  $S_Q$ ,  $S_K$ , and  $S_V$  are the firing rates of query, key, and value respectively.

| Method    | Complexity           | Energy Consumption                               |
|-----------|----------------------|--|
| ViT [11]  | $\mathcal{O}(N^2D)$  | $E_{MAC} \cdot N^2D$                             |
| T-STAtten | $\mathcal{O}(TND^2)$ | $E_{AC} \cdot TND^2 \cdot (S_K \cdot S_V + S_Q)$ |
| N-STAtten | $\mathcal{O}(T^2ND)$ | $E_{AC} \cdot T^2ND \cdot (S_Q \cdot S_K + S_V)$ |

location of patches, as shown in Fig. 4(c). The key distinction with T-STAtten is that N-STAtten calculates attention scores between different indexes of patches while considering all timesteps during calculation. The formulation for N-STAtten is as follows:

$$\mathbf{C}_1 = (\mathbf{Q}_1 \odot \mathbf{K}_2^\top), \mathbf{C}_2 = (\mathbf{Q}_2 \odot \mathbf{K}_1^\top), \quad \mathbf{C}_{1,2} \in \mathbb{R}^{\frac{N}{2} \times T \times T} \quad (7)$$

$$\text{Attn} = \text{Avg}_n(\text{Concat}_n(\mathbf{C}_1, \mathbf{C}_2)) \quad \text{Attn} \in \mathbb{R}^{T \times T} \quad (8)$$

$$\mathbf{O} = \alpha \cdot (\text{Attn} \odot \mathbf{V}) \quad \mathbf{O} \in \mathbb{R}^{T \times N \times D}, \quad (9)$$

where  $\text{Avg}_n$  and  $\text{Concat}_n$  represent averaging and concatenate function across the token dimension respectively. We use  $\mathbf{Q}$  and  $\mathbf{K}$  for the first multiplication to decrease the computational complexity, *i.e.*,  $\mathcal{O}(T^2ND)$ . Given that we often use 4 or 6 timesteps for image datasets, this results in significantly lower complexity during attention calculation compared to other attention methods.

### 4.3 Attention Complexity and Energy consumption

In this section, we clarify how to calculate the computational complexity and theoretical energy consumption of our proposed architecture. Here, we consider complexity and energy only for the self-attention part, and other evaluated values on the overall architecture are elaborated in the Appendix B. In Table 1, the complexity represents the computational complexity of matrix multiplication between  $\mathbf{Q}$  and  $\mathbf{K}$  or  $\mathbf{K}$  and  $\mathbf{V}$ . For energy consumption, we estimate the energy cost with floating-point operations (FLOPs) implementation in 45nm technology [35].  $E_{MAC}$  represents the energy cost for multiply-accumulate operation (MAC) corresponding to 32-bit ANN operation, while  $E_{AC}$  is for accumulate operation (AC) used for binary calculation in SNN.  $S_Q$ ,  $S_K$ , and  $S_V$  denote the firing rates of  $\mathbf{Q}$ ,  $\mathbf{K}$ , and  $\mathbf{V}$ , respectively, which are multiplied with  $E_{MAC}$  or  $E_{AC}$  for the final energy cost. We will analyze the energy results in Section 5.3.

## 5 Experiments

We verify our proposed methods on both static and dynamic datasets, *e.g.*, CIFAR10/100 [36], ImageNet [37], CIFAR10-DVS [38], and N-Caltech101 [39] datasets. We adopt SDT architecture [16] as our baseline and apply our spatial-temporal attention modules. We use direct coding to convert float pixel values into binary spikes [6] and all experiments are trained from scratch. The detailed training strategy for each dataset is explained in the Appendix C.

### 5.1 Temporal Dependency Analysis

Inspired by [40], we first validate the capability for the long-term temporal dependency of our proposed spatial-temporal attention mechanism on sequential CIFAR10 and CIFAR100 datasets. In these datasets, the original input images, which are typically used for image classification tasks, are divided column-by-column. Each column is used as input for one timestep. Therefore, for CIFAR10/100, the number of timesteps is 32, corresponding to the width of the image. This experiment with sequential dataset allows us to evaluate how well a network can capture temporal correlation and learn long-term dependency. Consequently, we expect that our spatial-temporal attention mechanisms will outperform the SDT architecture, which uses only spatial attention. To accommodate the 1-D input of the sequential dataset, we modify our convolutional, batch normalization, and pooling layers from 2-D to 1-D.

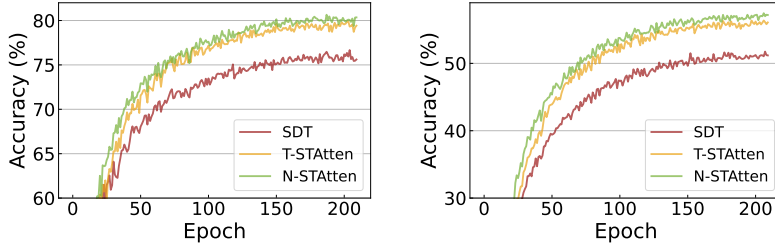


Figure 5: Accuracy-epoch curves of different self-attention methods on sequential (a) CIFAR10 and (b) CIFAR100 datasets.

Table 2 and Fig. 5 show the accuracy and accuracy curves of the SDT and STatten methods on sequential CIFAR10/100 datasets. As expected, the accuracy of all our STatten methods is higher than that of the SDT architecture, which uses only spatial self-attention. Specifically, N-STatten achieves an accuracy improvement of 3.98 % on CIFAR10 and 5.70 % on CIFAR100 compared to SDT. Additionally, we observe that the results of T-STatten are lower than those of the N-STatten method. We believe this is because, although long-term temporal dependency is crucial in sequential classification tasks, the ability of T-STatten to capture this dependency is hindered due to the division across the timestep in its calculation. In contrast, N-STatten calculates the temporal correlation across every timestep. Through this sequential data experiment, we can conclude that integrating spatial-temporal attention significantly enhances the performance of spiking transformers in tasks requiring temporal dependency.

Table 2: Accuracy comparison SDT and our STatten on sequential CIFAR10/100 dataset.

| Method    | CIFAR10 (%) | CIFAR100 (%) |
|-----------|-------------|--------------|
| SDT [16]  | 76.67       | 51.75        |
| T-STatten | 79.92       | 56.37        |
| N-STatten | 80.65       | 57.45        |

## 5.2 Performance Analysis

**CIFAR10/100.** CIFAR10/100 are datasets consisting of static images with dimensions of  $32 \times 32$  pixels and comprise 50,000 training images and 10,000 test images. As demonstrated in Table 3, our T-STatten method achieves accuracies of 95.83 % and 79.50 % on CIFAR10 and CIFAR100, respectively, surpassing the performance of Spikformer and SDT. Specifically, our T-STatten and N-STatten methods achieve accuracy improvements of 1.10 %, and 0.61 % over SDT on the CIFAR100 dataset, respectively. This indicates that attention across the time dimension is crucial for transformer-based SNNs.

**ImageNet.** ImageNet is a large-scale image dataset with images sized  $224 \times 224$  pixels, comprising approximately 1.2 million training images and 50,000 validation images across 1,000 classes. To ensure a fair comparison, we follow the experimental setup in [16] and replace the self-attention mechanism with our methods, *e.g.*, T-STatten, and N-STatten. The experimental results on the ImageNet dataset are presented in Table 4. Our methods initially achieve superior accuracy compared to other convolution-based architectures. Specifically, in the spiking transformer architecture, our

Table 3: Performance comparison between our methods and previous works on CIFAR10 and CIFAR100 datasets. In the architecture column,  $L$ - $D$  represents  $L$  number of encoder blocks and  $D$  hidden dimensions.

| Method          | Architecture     | Timestep | CIFAR10 (%)  | CIFAR100 (%) |
|-----------------|------------------|----------|--------------|--------------|
| tdBN [8]        | ResNet19         | 4        | 92.92        | -            |
| PLIF [41]       | ConvNet          | 8        | 93.50        | -            |
| Dspike [42]     | ResNet18         | 6        | 94.25        | 74.24        |
| DSR [43]        | ResNet18         | 20       | 95.40        | 78.50        |
| DIET-SNN [44]   | VGG16            | 5        | 92.70        | 69.67        |
| SNASNet [45]    | ConvNet          | 5        | 93.64        | 73.04        |
| Spikformer [15] | Spikformer-4-384 | 4        | 95.50        | 78.20        |
| SDT [16]        | SDT-2-512        | 4        | 95.60        | 78.40        |
| T-STatten       | SDT-2-512        | 4        | <b>95.83</b> | <b>79.50</b> |
| N-STatten       | SDT-2-512        | 4        | 95.30        | 79.01        |

Table 4: Performance comparison between our methods and previous works on ImageNet datasets. Note that \* represents the inference accuracy with  $288 \times 288$  resolution. In the architecture column,  $L$ - $D$  represents  $L$  number of encoder blocks and  $D$  hidden dimensions.

| Method              | Architecture      | Param(M) | Timestep | Accuracy(%)           |
|---------------------|-------------------|----------|----------|-----------------------|
| TET [46]            | SEW-ResNet34      | 21.79    | 4        | 68.00                 |
| Spiking ResNet [47] | ResNet50          | 25.56    | 350      | 72.75                 |
| tdBN [8]            | ResNet34          | 21.79    | 6        | 63.72                 |
| SEW-ResNet [29]     | SEW-ResNet152     | 60.19    | 4        | 69.26                 |
| MS-ResNet [9]       | ResNet104         | 78.37    | 5        | 74.21 / 76.02*        |
| Att-MS-ResNet [48]  | ResNet104         | 78.37    | 4        | 77.08*                |
| -----               |                   |          |          |                       |
| Spikformer [15]     | Spikformer-8-512  | 29.68    | 4        | 73.38                 |
|                     | Spikformer-10-512 | 36.01    | 4        | 73.68                 |
|                     | Spikformer-8-768  | 66.34    | 4        | 74.81                 |
| -----               |                   |          |          |                       |
| SDT [16]            | SDT-8-512         | 29.68    | 4        | 74.57                 |
|                     | SDT-10-512        | 36.01    | 4        | 74.66                 |
|                     | SDT-8-768         | 66.34    | 4        | 76.32 / 77.07*        |
| -----               |                   |          |          |                       |
| T-STAtten           | SDT-8-512         | 29.68    | 4        | 76.18 / 76.56*        |
|                     | SDT-8-768         | 66.34    | 4        | <b>78.11 / 78.39*</b> |
| N-STAtten           | SDT-8-768         | 66.34    | 4        | 77.31 / 77.86*        |

Table 5: Performance comparison between our methods and previous works on CIFAR10-DVS and N-Caltech101 datasets. † represents our implementation. In the architecture column,  $L$ - $D$  represents  $L$  number of encoder blocks and  $D$  hidden dimensions.

| Method          | Architecture     | Timestep | CIFAR10-DVS (%) | N-Caltech101 (%) |
|-----------------|------------------|----------|-----------------|------------------|
| tdBN [8]        | ResNet19         | 10       | 67.80           | -                |
| PLIF [41]       | ConvNet          | 20       | 74.80           | -                |
| Dspike [42]     | ResNet18         | 10       | 75.40           | -                |
| DSR [43]        | ResNet18         | 20       | 77.27           | -                |
| SEW-ResNet [29] | ConvNet          | 20       | 74.80           | -                |
| TT-SNN [49]     | ResNet34         | 6        | -               | 77.80            |
| NDA [50]        | VGG11            | 10       | 79.6            | 78.2             |
| -----           |                  |          |                 |                  |
| Spikformer [15] | Spikformer-2-256 | 16       | 80.9            | -                |
| SDT [16]        | SDT-2-256        | 16       | 80.0            | 81.80 †          |
| T-STAtten       | SDT-2-256        | 16       | <b>82.2</b>     | <b>84.36</b>     |

T-STAtten method with a resolution of  $224 \times 224$  achieves 3.30 % and 1.79 % higher accuracy than Spikformer [15] and SDT [16], respectively, for the same number of trainable parameters. With an increased resolution of  $288 \times 288$ , we achieve an accuracy of 78.39 % using the T-STAtten method. The N-STAtten method achieves an accuracy of 77.31 %, still outperforming our baseline. These results indicate that replacing traditional spatial attention with spatial-temporal attention significantly improves performance in spiking transformers, highlighting the importance of capturing spatial-temporal correlations during the training of spiking transformers.

**Neuromorphic dataset.** For the experiments on neuromorphic datasets, we utilize CIFAR10-DVS [38] and N-Caltech101 [39]. CIFAR10-DVS is obtained from static images through a Dynamic Vision Sensor (DVS), comprising 10,000 samples which are divided into 9,000 training and 1,000 testing samples. N-Caltech101 is derived from the Caltech101 dataset [51], consisting of 8,831 DVS image samples. We resize the CIFAR10-DVS samples to  $64 \times 64$  and apply the same augmentation strategy as used for SDT [16]. For the N-Caltech101 dataset, we resize it to  $64 \times 64$  and employ NDA [50] augmentation. The results for the neuromorphic dataset are presented in Table 5, and our results are obtained with the T-STAtten method. The accuracy achieved on CIFAR10-DVS is 82.2 %, surpassing the performance of Spikformer by 1.3 % and SDT by 2.2 %. Moreover, on the N-Caltech101 dataset, our method achieves an accuracy that is 2.56 % higher than that of the SDT.

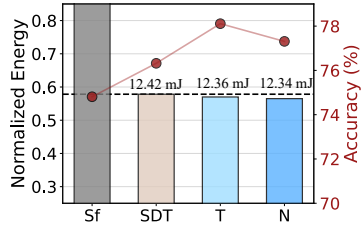


Figure 6: Comparison of energy consumption between the several spiking transformers. Sf, T, N represent Spikformer [15], T-STAtten, and N-STAtten respectively. The dashed line represents the normalized energy of the SDT.

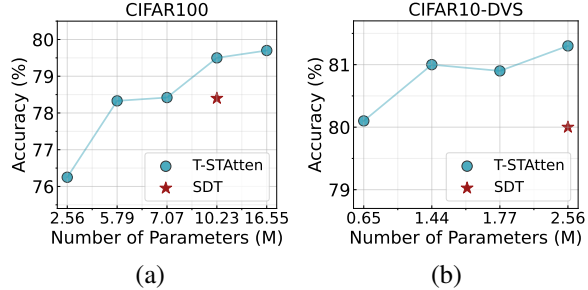


Figure 7: Accuracy comparison with respect to the number of parameters on (a) CIFAR10 and (b) CIFAR10-DVS datasets. The architecture is 2-256 (# Encoder-# Channel) of SDT, and the T-STAtten method is used.

### 5.3 Theoretical Energy Consumption Analysis

As discussed in Section 4.3, we calculate the theoretical energy consumption of our methods and compare them to previous spiking transformers. In Fig.6, we compare against Spikformer [15] and SDT [16]. The energy is calculated during inference with the  $224 \times 224$  ImageNet dataset on the 8-768 architecture. We normalize the energy of the Spikformer as 1.0 and calculate the relative normalized energy of other methods. The normalized energy of the SDT is 0.58, while the energy of our T-STAtten and N-STAtten methods are 0.57, and 0.56 respectively. Interestingly, our proposed methods exhibit a lower energy consumption to SDT during inference. This theoretical energy calculation supports that our spatial-temporal attentions achieve superior performance with lower energy consumption. The detailed calculation equations of the whole architecture are provided in the Appendix B.

### 5.4 Model Capacity

To further evaluate the capacity of our spatial-temporal attention methods in spiking transformer, we compare the accuracy based on the number of trainable parameters through ablation studies. The Fig. 7 (a) and (b) show the accuracy on CIFAR100 and CIFAR10-DVS datasets respectively, using various architectures. Our baseline is the SDT, and the T-STAtten attention method is employed for our results. On CIFAR100, with the same architecture (10.23 M parameters), our spatial-temporal attention achieves higher accuracy than our baseline and maintains similar accuracy even with a  $2 \times$  smaller architecture. Moreover, on the CIFAR10-DVS dataset, our method achieves comparable performance to the baseline with a significantly smaller architecture, approximately  $4 \times$  smaller.

## 6 Conclusion

Even though varied spike patterns exist in  $Q$ ,  $K$ , and  $V$  of spiking transformers, previous works have primarily focused on spatial self-attention. To address this, we propose three spatial-temporal self-attention methods, T-STAtten, and N-STAtten, which effectively capture the diverse spike patterns across timesteps. Our extensive experiments on both static and dynamic datasets validate the capacity and efficiency of our proposed methods, highlighting the importance of spatial-temporal correlation in the self-attention of spiking transformers. Furthermore, through experiments with sequential datasets, we verify that our spatial-temporal attention methods can effectively learn long-term temporal dependencies.

## References

- [1] Wolfgang Maass. Networks of spiking neurons: the third generation of neural network models. *Neural networks*, 10(9):1659–1671, 1997.
- [2] Kaushik Roy, Akhilesh Jaiswal, and Priyadarshini Panda. Towards spike-based machine intelligence with neuromorphic computing. *Nature*, 575(7784):607–617, 2019.

- [3] Filipp Akopyan, Jun Sawada, Andrew Cassidy, Rodrigo Alvarez-Icaza, John Arthur, Paul Merolla, Nabil Imam, Yutaka Nakamura, Pallab Datta, Gi-Joon Nam, et al. Truenorth: Design and tool flow of a 65 mw 1 million neuron programmable neurosynaptic chip. *IEEE transactions on computer-aided design of integrated circuits and systems*, 34(10):1537–1557, 2015.
- [4] Mike Davies, Narayan Srinivasa, Tsung-Han Lin, Gautham Chinya, Yongqiang Cao, Sri Harsha Choday, Georgios Dimou, Prasad Joshi, Nabil Imam, Shweta Jain, et al. Loihi: A neuromorphic manycore processor with on-chip learning. *Ieee Micro*, 38(1):82–99, 2018.
- [5] Jing Pei, Lei Deng, Sen Song, Mingguo Zhao, Youhui Zhang, Shuang Wu, Guanrui Wang, Zhe Zou, Zhenzhi Wu, Wei He, et al. Towards artificial general intelligence with hybrid tianjic chip architecture. *Nature*, 572(7767):106–111, 2019.
- [6] Yujie Wu, Lei Deng, Guoqi Li, Jun Zhu, Yuan Xie, and Luping Shi. Direct training for spiking neural networks: Faster, larger, better. In *Proceedings of the AAAI conference on artificial intelligence*, volume 33, pages 1311–1318, 2019.
- [7] Abhronil Sengupta, Yuting Ye, Robert Wang, Chiao Liu, and Kaushik Roy. Going deeper in spiking neural networks: Vgg and residual architectures. *Frontiers in neuroscience*, 13:95, 2019.
- [8] Hanle Zheng, Yujie Wu, Lei Deng, Yifan Hu, and Guoqi Li. Going deeper with directly-trained larger spiking neural networks. In *Proceedings of the AAAI conference on artificial intelligence*, volume 35, pages 11062–11070, 2021.
- [9] Yifan Hu, Lei Deng, Yujie Wu, Man Yao, and Guoqi Li. Advancing spiking neural networks toward deep residual learning. *IEEE Transactions on Neural Networks and Learning Systems*, 2024.
- [10] Ashish Vaswani, Noam Shazeer, Niki Parmar, Jakob Uszkoreit, Llion Jones, Aidan N Gomez, Łukasz Kaiser, and Illia Polosukhin. Attention is all you need. *Advances in neural information processing systems*, 30, 2017.
- [11] Alexey Dosovitskiy, Lucas Beyer, Alexander Kolesnikov, Dirk Weissenborn, Xiaohua Zhai, Thomas Unterthiner, Mostafa Dehghani, Matthias Minderer, Georg Heigold, Sylvain Gelly, et al. An image is worth 16x16 words: Transformers for image recognition at scale. *arXiv preprint arXiv:2010.11929*, 2020.
- [12] Anurag Arnab, Mostafa Dehghani, Georg Heigold, Chen Sun, Mario Lučić, and Cordelia Schmid. Vivit: A video vision transformer. In *Proceedings of the IEEE/CVF international conference on computer vision*, pages 6836–6846, 2021.
- [13] Lili Chen, Kevin Lu, Aravind Rajeswaran, Kimin Lee, Aditya Grover, Misha Laskin, Pieter Abbeel, Aravind Srinivas, and Igor Mordatch. Decision transformer: Reinforcement learning via sequence modeling. *Advances in neural information processing systems*, 34:15084–15097, 2021.
- [14] Jiqing Zhang, Bo Dong, Haiwei Zhang, Jianchuan Ding, Felix Heide, Baocai Yin, and Xin Yang. Spiking transformers for event-based single object tracking. In *Proceedings of the IEEE/CVF conference on Computer Vision and Pattern Recognition*, pages 8801–8810, 2022.
- [15] Zhaokun Zhou, Yuesheng Zhu, Chao He, Yaowei Wang, Shuicheng Yan, Yonghong Tian, and Li Yuan. Spikformer: When spiking neural network meets transformer. *arXiv preprint arXiv:2209.15425*, 2022.
- [16] Man Yao, Jiakui Hu, Zhaokun Zhou, Li Yuan, Yonghong Tian, Bo Xu, and Guoqi Li. Spike-driven transformer. *Advances in Neural Information Processing Systems*, 36, 2024.
- [17] Jiyuan Zhang, Lulu Tang, Zhaofei Yu, Jiwen Lu, and Tiejun Huang. Spike transformer: Monocular depth estimation for spiking camera. In *European Conference on Computer Vision*, pages 34–52. Springer, 2022.

- [18] Zhengkun Tian, Jiangyan Yi, Jianhua Tao, Ye Bai, Shuai Zhang, and Zhengqi Wen. Spike-triggered non-autoregressive transformer for end-to-end speech recognition. *arXiv preprint arXiv:2005.07903*, 2020.
- [19] Qingyu Wang, Tielin Zhang, Minglun Han, Yi Wang, Duzhen Zhang, and Bo Xu. Complex dynamic neurons improved spiking transformer network for efficient automatic speech recognition. In *Proceedings of the AAAI Conference on Artificial Intelligence*, volume 37, pages 102–109, 2023.
- [20] Youngeun Kim, Yuhang Li, Hyoungeob Park, Yeshwanth Venkatesha, Anna Hambitzer, and Priyadarshini Panda. Exploring temporal information dynamics in spiking neural networks. In *Proceedings of the AAAI Conference on Artificial Intelligence*, volume 37, pages 8308–8316, 2023.
- [21] Yuhang Li, Youngeun Kim, Hyoungeob Park, and Priyadarshini Panda. Uncovering the representation of spiking neural networks trained with surrogate gradient. *arXiv preprint arXiv:2304.13098*, 2023.
- [22] Gedas Bertasius, Heng Wang, and Lorenzo Torresani. Is space-time attention all you need for video understanding? In *ICML*, volume 2, page 4, 2021.
- [23] Shikuang Deng and Shi Gu. Optimal conversion of conventional artificial neural networks to spiking neural networks. *arXiv preprint arXiv:2103.00476*, 2021.
- [24] Peter U Diehl et al. Fast-classifying, high-accuracy spiking deep networks through weight and threshold balancing. In *2015 International joint conference on neural networks (IJCNN)*, pages 1–8. iee, 2015.
- [25] Bing Han and Kaushik Roy. Deep spiking neural network: Energy efficiency through time based coding. In *European Conference on Computer Vision*, pages 388–404. Springer, 2020.
- [26] Yuhang Li, Shikuang Deng, Xin Dong, Ruihao Gong, and Shi Gu. A free lunch from ann: Towards efficient, accurate spiking neural networks calibration. In *International conference on machine learning*, pages 6316–6325. PMLR, 2021.
- [27] Sumit B Shrestha and Garrick Orchard. Slayer: Spike layer error reassignment in time. *Advances in neural information processing systems*, 31, 2018.
- [28] Sayeed Shafayet Chowdhury, Isha Garg, and Kaushik Roy. Spatio-temporal pruning and quantization for low-latency spiking neural networks. In *2021 International Joint Conference on Neural Networks (IJCNN)*, pages 1–9. IEEE, 2021.
- [29] Wei Fang, Zhaofei Yu, Yanqi Chen, Tiejun Huang, Timothée Masquelier, and Yonghong Tian. Deep residual learning in spiking neural networks. *Advances in Neural Information Processing Systems*, 34:21056–21069, 2021.
- [30] Youngeun Kim, Joshua Chough, and Priyadarshini Panda. Beyond classification: Directly training spiking neural networks for semantic segmentation. *Neuromorphic Computing and Engineering*, 2(4):044015, 2022.
- [31] Qiaoyi Su, Yuhong Chou, Yifan Hu, Jianing Li, Shijie Mei, Ziyang Zhang, and Guoqi Li. Deep directly-trained spiking neural networks for object detection. In *Proceedings of the IEEE/CVF International Conference on Computer Vision*, pages 6555–6565, 2023.
- [32] Anthony N Burkitt. A review of the integrate-and-fire neuron model: I. homogeneous synaptic input. *Biological cybernetics*, 95:1–19, 2006.
- [33] Ramprasaath R Selvaraju, Michael Cogswell, Abhishek Das, Ramakrishna Vedantam, Devi Parikh, and Dhruv Batra. Grad-cam: Visual explanations from deep networks via gradient-based localization. In *Proceedings of the IEEE international conference on computer vision*, pages 618–626, 2017.
- [34] Youngeun Kim, Yuhang Li, Hyoungeob Park, Yeshwanth Venkatesha, Ruokai Yin, and Priyadarshini Panda. Exploring lottery ticket hypothesis in spiking neural networks. In *European Conference on Computer Vision*, pages 102–120. Springer, 2022.

- [35] Mark Horowitz. 1.1 computing’s energy problem (and what we can do about it). In *2014 IEEE international solid-state circuits conference digest of technical papers (ISSCC)*, pages 10–14. IEEE, 2014.
- [36] Alex Krizhevsky, Geoffrey Hinton, et al. Learning multiple layers of features from tiny images. 2009.
- [37] Jia Deng, Wei Dong, Richard Socher, Li-Jia Li, Kai Li, and Li Fei-Fei. Imagenet: A large-scale hierarchical image database. In *2009 IEEE conference on computer vision and pattern recognition*, pages 248–255. Ieee, 2009.
- [38] Hongmin Li, Hanchao Liu, Xiangyang Ji, Guoqi Li, and Luping Shi. Cifar10-dvs: an event-stream dataset for object classification. *Frontiers in neuroscience*, 11:244131, 2017.
- [39] Garrick Orchard, Ajinkya Jayawant, Gregory K Cohen, and Nitish Thakor. Converting static image datasets to spiking neuromorphic datasets using saccades. *Frontiers in neuroscience*, 9:159859, 2015.
- [40] Wei Fang, Zhaofei Yu, Zhaokun Zhou, Ding Chen, Yanqi Chen, Zhengyu Ma, Timothée Masquelier, and Yonghong Tian. Parallel spiking neurons with high efficiency and ability to learn long-term dependencies. *Advances in Neural Information Processing Systems*, 36, 2024.
- [41] Wei Fang, Zhaofei Yu, Yanqi Chen, Timothée Masquelier, Tiejun Huang, and Yonghong Tian. Incorporating learnable membrane time constant to enhance learning of spiking neural networks. In *Proceedings of the IEEE/CVF international conference on computer vision*, pages 2661–2671, 2021.
- [42] Yuhang Li, Yufei Guo, Shanghang Zhang, Shikuang Deng, Yongqing Hai, and Shi Gu. Differentiable spike: Rethinking gradient-descent for training spiking neural networks. *Advances in Neural Information Processing Systems*, 34:23426–23439, 2021.
- [43] Qingyan Meng, Mingqing Xiao, Shen Yan, Yisen Wang, Zhouchen Lin, and Zhi-Quan Luo. Training high-performance low-latency spiking neural networks by differentiation on spike representation. In *Proceedings of the IEEE/CVF Conference on Computer Vision and Pattern Recognition*, pages 12444–12453, 2022.
- [44] Nitin Rathi and Kaushik Roy. Diet-snn: Direct input encoding with leakage and threshold optimization in deep spiking neural networks. *arXiv preprint arXiv:2008.03658*, 2020.
- [45] Youngeun Kim, Yuhang Li, Hyoungseob Park, Yeshwanth Venkatesha, and Priyadarshini Panda. Neural architecture search for spiking neural networks. In *European Conference on Computer Vision*, pages 36–56. Springer, 2022.
- [46] Shikuang Deng, Yuhang Li, Shanghang Zhang, and Shi Gu. Temporal efficient training of spiking neural network via gradient re-weighting. *arXiv preprint arXiv:2202.11946*, 2022.
- [47] Yangfan Hu, Huajin Tang, and Gang Pan. Spiking deep residual networks. *IEEE Transactions on Neural Networks and Learning Systems*, 34(8):5200–5205, 2021.
- [48] Man Yao, Guangshe Zhao, Hengyu Zhang, Yifan Hu, Lei Deng, Yonghong Tian, Bo Xu, and Guoqi Li. Attention spiking neural networks. *IEEE transactions on pattern analysis and machine intelligence*, 2023.
- [49] Donghyun Lee, Ruokai Yin, Youngeun Kim, Abhishek Moitra, Yuhang Li, and Priyadarshini Panda. Tt-snn: Tensor train decomposition for efficient spiking neural network training. *arXiv preprint arXiv:2401.08001*, 2024.
- [50] Yuhang Li, Youngeun Kim, Hyoungseob Park, Tamar Geller, and Priyadarshini Panda. Neuro-morphic data augmentation for training spiking neural networks. In *European Conference on Computer Vision*, pages 631–649. Springer, 2022.
- [51] FF Li, M Andreeto, M Ranzato, and P Perona. Caltech 101 (1.0)[data set]. caltechdata, 2022.

- [52] Peihao Wang, Wenqing Zheng, Tianlong Chen, and Zhangyang Wang. Anti-oversmoothing in deep vision transformers via the fourier domain analysis: From theory to practice. *arXiv preprint arXiv:2203.05962*, 2022.
- [53] Namuk Park and Songkuk Kim. How do vision transformers work? *arXiv preprint arXiv:2202.06709*, 2022.
- [54] Rulin Shao, Zhouxing Shi, Jinfeng Yi, Pin-Yu Chen, and Cho-Jui Hsieh. On the adversarial robustness of vision transformers. *arXiv preprint arXiv:2103.15670*, 2021.
- [55] Namuk Park and Songkuk Kim. Blurs behave like ensembles: Spatial smoothings to improve accuracy, uncertainty, and robustness. In *International Conference on Machine Learning*, pages 17390–17419. PMLR, 2022.

## A Overall Architecture

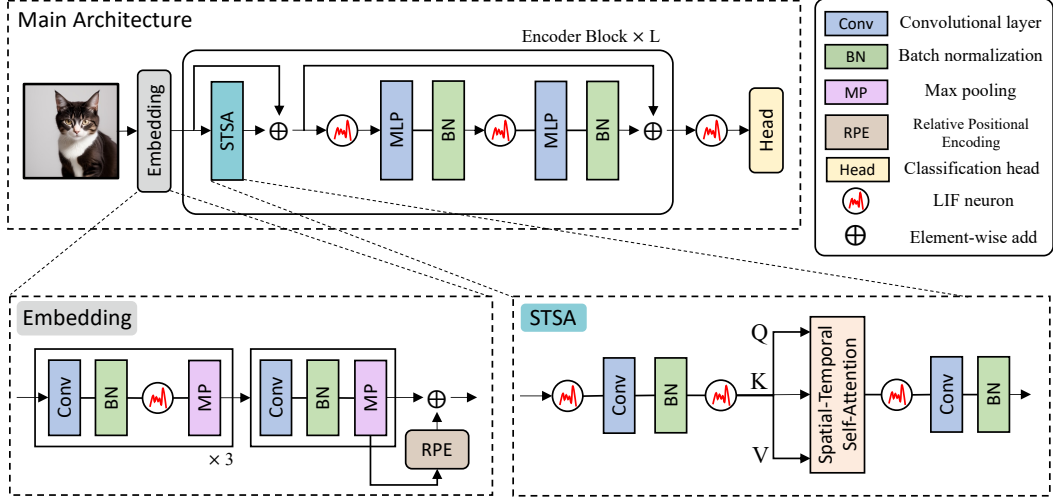


Figure 8: Overall architecture of STAtten. Our model is based on SDT [16]. In the Spatial-Temporal Self-Attention (STSA) block, we use spatial-temporal attention modules, *e.g.*, T-STAtten, and N-STAtten.

In this section, we present the holistic architecture of our STAtten model, which is based on the SDT architecture [16]. In the embedding block, five convolutional layers with batch normalization (BN) and max pooling (MP) split the input images into spike-formed  $N$  patches. In the Spatial-Temporal Self-Attention (STSA) block, after obtaining spike-formed  $Q$ ,  $K$ , and  $V$  through linear projection, we calculate the spatial-temporal attention using our proposed methods: T-STAtten, and N-STAtten. Following  $L$  iterations of the encoder block, we compute the logits through the classification head. Our residual connections adhere to the MS-ResNet rule [9].

## B Energy Calculation Details

To clarify the energy consumption of our STAtten architecture in Section 5.3, we present the detailed equations of every layer shown in Table 6.

Table 6: The detailed equations of energy consumption on every layer of STAtten architecture.

| Block     | Layer          | Energy Consumption                                     |
|-----------|----------------|--|
| Embedding | First Conv     | $E_{MAC} \cdot F_{Conv} \cdot T$                       |
|           | Other Convs    | $E_{AC} \cdot F_{Conv} \cdot T \cdot S_{Conv}$         |
| STSA      | $Q, K, V$      | $3 \cdot E_{AC} \cdot F_{Conv} \cdot T \cdot S_{Conv}$ |
|           | Self-attention | $E_{AC} \cdot TN D^2 \cdot (S_K \cdot S_V + S_Q)$      |
| MLP       | MLP            | $E_{AC} \cdot F_{Conv} \cdot T \cdot S_{Conv}$         |
|           | MLP1           | $E_{AC} \cdot F_{Conv} \cdot T \cdot S_{Conv}$         |
|           | MLP2           | $E_{AC} \cdot F_{Conv} \cdot T \cdot S_{Conv}$         |

Here,  $E_{MAC}$  is the energy of MAC operation,  $F_{Conv}$  is FLOPs of the convolutional layer,  $T$ ,  $N$ , and  $D$  are timestep, the number of patches, and channel dimension respectively,  $S_{Conv}$  is the firing rate of input spikes on the convolutional layer,  $S_Q$ ,  $S_K$ , and  $S_V$  are the firing rate of input spikes on  $Q$ ,  $K$ , and  $V$  projection layer respectively. The FLOPs of the convolutional layer can be calculated as follows:

$$F_{Conv} = K \cdot K \cdot H_{out} \cdot W_{out} \cdot C_{in} \cdot C_{out}, \quad (10)$$

where  $K$  is kernel size,  $H_{out}$  and  $W_{out}$  are the height and width of the output feature map respectively, and  $C_{in}$  and  $C_{out}$  are the input and output channel dimension respectively.

In the embedding block, for the first convolutional layer, since we use direct coding to convert a float pixel value into binary spikes [6], the firing rate does not need to be calculated for energy consumption, and  $E_{MAC}$  is used for the float pixel input. In the STSA block, for the energy calculation of the self-attention part, we can use the equations of our spatial-temporal methods shown in Table 1. Following previous works [15, 16], we calculate the energy consumption based on the FLOPs operation executed in 45nm CMOS technology [35], *e.g.*,  $E_{MAC} = 4.6pJ$ , and  $E_{AC} = 0.9pJ$ . The calculated values of the firing rate and the theoretical energy consumption of the T-STAtten method are provided in Appendix E.

## C Experimental Details

In this section, we provide the experimental details on CIFAR10/100, ImageNet, CIFAR10-DVS, and N-Caltech101 datasets in Table 7. We follow the general experimental setup in [16].

Table 7: The experimental details on each dataset.  $L$ - $D$  in architecture represents  $L$  number of encoder blocks and  $D$  channel dimension.

|                | CIFAR10/100 | ImageNet | CIFAR10-DVS | N-Caltech101 |
|----------------|-------------|----------|-------------|--------------|
| Timestep       | 4           | 4        | 16          | 16           |
| Batch size     | 64          | 32       | 16          | 16           |
| Learning rate  | 0.0003      | 0.001    | 0.01        | 0.01         |
| Training epoch | 310         | 210      | 210         | 210          |
| Optimizer      | AdamW       | Lamb     | AdamW       | AdamW        |
| Hardware (GPU) | A5000       | A100     | A5000       | A5000        |
| Architecture   | 2-512       | 8-768    | 2-256       | 2-256        |

We apply data augmentation following [15, 16]. For the ImageNet dataset, general augmentation techniques such as random augmentation, mixup, and cutmix are employed. Different data augmentation strategies are applied to the CIFAR10-DVS and N-Caltech101 datasets according to NDA [50]. While training on the dynamic datasets, we add a pooling layer branch and a residual connection to the spatial-temporal attention layer. The outputs of the pooling layer and the spatial-temporal attention are then multiplied element-wise to extract important spike feature maps.

## D Robustness

In this section, we investigate and evaluate the spiking transformer in the Fourier space. In [52, 53], the authors showed that the self-attention mechanism in ViT [11] acts as a low-pass filter, preserving primarily low-frequency signals across layers. Interestingly, our investigation indicates that the spiking transformer behaves as a high-pass filter, gradually eliminating low-frequency signals. To clarify the characteristics of the spiking transformer in the frequency domain, we compare the Relative Log Amplitude (RLA) of the Fourier transformed feature map between ViT-Base [11] and our pre-trained T-STAtten method. The RLA quantifies the difference in log amplitude at normalized frequencies  $0.0\pi$  and  $1.0\pi$ , corresponding to the center and boundary of the image, respectively. We follow the setup in [53] to obtain RLA results. As depicted in Fig.9 (a), while the RLA of ViT-Base steadily decreases through the layers, indicating the preservation of low-frequency components, our model exhibits the opposite trend, erasing low-frequency signals.

To further validate our findings, we assess the impact of noise perturbations with various frequency ranges on model accuracy, *e.g.*,  $0.1\pi$  to  $0.9\pi$ . Similar to [54, 55, 53], we add noise to images via Fourier transformation as follows:  $x_p = x_0 + f^{-1}(f(n) \odot M_f)$ , where  $x_p$  represents the perturbed images,  $x_0$  denotes the original noise-free image,  $f$  and  $f^{-1}$  denote the Fourier transform and inverse Fourier transform,  $n$  denotes frequency-based random noise, and  $M_f$  represents the frequency mask. This perturbation process yields noised data, as illustrated in Fig.9 (b). Leveraging the insights from Fig.9 (a), we anticipate that ViT may be susceptible to low-frequency noise, while our STAtten model is vulnerable to high-frequency noise. Indeed, Fig.9 (c) confirms that ViT-Base exhibits robustness to high-frequency noise but is sensitive to low-frequency noise, while our T-STAtten model displays the opposite behavior. When the frequency of noise is low, *i.e.*,  $0.1\pi$ , the accuracy

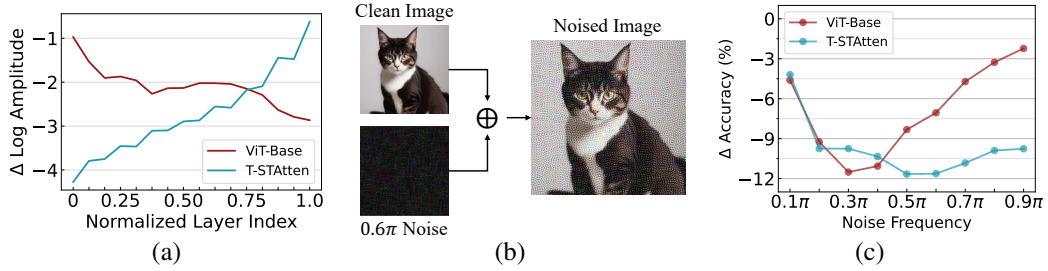


Figure 9: (a) The Relative Log Amplitude (RLA) of Fourier transformed feature map between ViT-Base and our proposed method. RLA represents the difference in log amplitude at normalized frequencies at  $0.0\pi$  (center) and  $1.0\pi$  (boundary). (b) The process of making a perturbed image. The noise at a specific frequency level can be obtained by a frequency mask. (c) The robustness comparison between ViT-Base and our model. The spiking transformer acts as a high-pass filter.

drop is -4.2 %. However, when the noise frequency exceeds  $0.2\pi$ , the accuracy drops around 10 %. This measurement indicates that the spiking transformer, particularly our T-STAtten architecture, functions as a high-pass filter and is robust against high-frequency noise.

## E Firing rate

In this section, we present the firing rate and energy consumption of each layer in 8-768 T-STAtten architecture pre-trained with the ImageNet dataset. Note that the firing rates represent the firing rate of input spikes for each layer. Additionally, for the firing rate of Self-attention in the table below, we calculate it using the equation:  $S_K \cdot S_V + S_Q$ .

| Block     | Layer          | $T = 1$ | $T = 2$ | $T = 3$ | $T = 4$ | Energy ( $mJ$ ) |
|-----------|----------------|---------|---------|---------|---------|-----------------|
| Embedding | 1st Conv       | -       | -       | -       | -       | 0.5982          |
|           | 2nd Conv       | 0.0771  | 0.1389  | 0.1092  | 0.1561  | 0.9015          |
|           | 3rd Conv       | 0.0424  | 0.0644  | 0.0586  | 0.0527  | 0.4089          |
|           | 4th Conv       | 0.0328  | 0.0501  | 0.0428  | 0.0480  | 0.3253          |
|           | 5th Conv       | 0.0660  | 0.1402  | 0.1308  | 0.1413  | 0.4478          |
| Encoder-1 | $Q, K, V$      | 0.2159  | 0.2662  | 0.2609  | 0.2728  | 0.3171          |
|           | Self-attention | 0.1221  | 0.1313  | 0.1320  | 0.1451  | 0.0551          |
|           | MLP            | 0.2018  | 0.2962  | 0.2880  | 0.3454  | 0.1177          |
| MLP-1     | MLP1           | 0.3292  | 0.3605  | 0.3622  | 0.3697  | 0.5916          |
|           | MLP2           | 0.0340  | 0.0409  | 0.0401  | 0.0458  | 0.0670          |
| Encoder-2 | $Q, K, V$      | 0.3268  | 0.3583  | 0.3543  | 0.3967  | 0.4482          |
|           | Self-attention | 0.0986  | 0.0950  | 0.0945  | 0.1017  | 0.0405          |
|           | MLP            | 0.2760  | 0.3532  | 0.3371  | 0.3511  | 0.1370          |
| MLP-2     | MLP1           | 0.3094  | 0.3332  | 0.3321  | 0.3718  | 0.5604          |
|           | MLP2           | 0.0226  | 0.0293  | 0.0301  | 0.0350  | 0.0487          |
| Encoder-3 | $Q, K, V$      | 0.3240  | 0.3462  | 0.3504  | 0.3917  | 0.4408          |
|           | Self-attention | 0.0752  | 0.0694  | 0.0680  | 0.0654  | 0.0289          |
|           | MLP            | 0.2837  | 0.3409  | 0.3254  | 0.2879  | 0.1288          |
| MLP-3     | MLP1           | 0.3486  | 0.3519  | 0.3588  | 0.3957  | 0.6056          |
|           | MLP2           | 0.0186  | 0.0241  | 0.0245  | 0.0255  | 0.0386          |
| Encoder-4 | $Q, K, V$      | 0.3532  | 0.3570  | 0.3661  | 0.4015  | 0.4613          |
|           | Self-attention | 0.0716  | 0.0707  | 0.0704  | 0.0743  | 0.0298          |
|           | MLP            | 0.2586  | 0.3299  | 0.3246  | 0.3203  | 0.1283          |
| MLP-4     | MLP1           | 0.3591  | 0.3544  | 0.3633  | 0.3965  | 0.6132          |
|           | MLP2           | 0.0138  | 0.0177  | 0.0183  | 0.0188  | 0.0286          |
| Encoder-5 | $Q, K, V$      | 0.3599  | 0.3588  | 0.3688  | 0.3979  | 0.4637          |
|           | Self-attention | 0.0701  | 0.0619  | 0.0610  | 0.0631  | 0.0266          |
|           | MLP            | 0.2695  | 0.2588  | 0.2469  | 0.2187  | 0.1034          |
| MLP-5     | MLP1           | 0.3645  | 0.3579  | 0.3691  | 0.3979  | 0.6199          |
|           | MLP2           | 0.0098  | 0.0126  | 0.0128  | 0.0134  | 0.0202          |
| Encoder-6 | $Q, K, V$      | 0.3737  | 0.3621  | 0.3706  | 0.3941  | 0.4684          |
|           | Self-attention | 0.0740  | 0.0581  | 0.0533  | 0.0496  | 0.0244          |
|           | MLP            | 0.2071  | 0.2260  | 0.1896  | 0.1393  | 0.0793          |
| MLP-6     | MLP1           | 0.3832  | 0.3665  | 0.3743  | 0.3963  | 0.6327          |
|           | MLP2           | 0.0108  | 0.0128  | 0.0119  | 0.0107  | 0.0193          |
| Encoder-7 | $Q, K, V$      | 0.3815  | 0.3665  | 0.3663  | 0.3826  | 0.4672          |
|           | Self-attention | 0.0746  | 0.0575  | 0.0538  | 0.0528  | 0.0248          |
|           | MLP            | 0.1802  | 0.1670  | 0.1362  | 0.0972  | 0.0604          |
| MLP-7     | MLP1           | 0.3773  | 0.3574  | 0.3549  | 0.3686  | 0.6069          |
|           | MLP2           | 0.0056  | 0.0068  | 0.0068  | 0.0063  | 0.0106          |
| Encoder-8 | $Q, K, V$      | 0.3772  | 0.3423  | 0.3471  | 0.3594  | 0.4452          |
|           | Self-attention | 0.1180  | 0.0853  | 0.0784  | 0.0728  | 0.0369          |
|           | MLP            | 0.1383  | 0.1324  | 0.1143  | 0.1010  | 0.0505          |
| MLP-8     | MLP1           | 0.3684  | 0.3480  | 0.3616  | 0.3818  | 0.6075          |
|           | MLP2           | 0.0123  | 0.0177  | 0.0168  | 0.0145  | 0.0255          |